Physics Open 8 (2021) 100077

Contents lists available at ScienceDirect

Physics Open

journal homepage: www.journals.elsevier.com/physics-open

Photoluminescence tuning in $Ba_3ScB_3O_9:Eu^{2+}$ phosphor by crystal-site engineering

Shunqi Lai [a], Tao Hu [a], Maxim S. Molokeev [b,c,d], Zhiguo Xia [a,*]

[a] State Key Laboratory of Luminescent Materials and Devices and Guangdong Provincial Key Laboratory of Fiber Laser Materials and Applied Techniques, South China University of Technology, Guangzhou, 510641, China
[b] Laboratory of Crystal Physics, Kirensky Institute of Physics, Federal Research Center KSC SB RAS, Krasnoyarsk, 660036, Russia
[c] Siberian Federal University, Krasnoyarsk, 660041, Russia
[d] Department of Physics, Far Eastern State Transport University, Khabarovsk, 680021, Russia

ARTICLE INFO

Keywords:
Phosphor
Photoluminescence tuning
Crystal-site engineering
Doping

ABSTRACT

Controlled photoluminescence tuning is essential for optimizing and accelerating the application of phosphor materials. Here, we adopt the crystal-site engineering method to tailor the photoluminescence properties in $Ba_3ScB_3O_9:Eu^{2+}$. $Ba_3ScB_3O_9$ host contains multiple cationic sites which help to finely regulate Eu^{2+} site occupancies and thus the emission color. The relationship between Eu^{2+} emission and the local environments has been analyzed, and we demonstrate that the emission colors of the phosphors can be widely tuned from NIR to yellow by chemically driving the Eu^{2+} from octahedrally-coordinated Sc^{3+} sites to nine-fold coordinated Ba^{2+} sites. Our study will initiate and guide more explorations on discovering new phosphors through crystal-site engineering.

1. Introduction

Phosphor-converted light-emitting diodes (pc-LEDs), featuring low cost, high energy utilization efficiency and long service life, are considered as a new generation light source [1,2]. New phosphors with high physical and chemical stability, appropriate absorption/emission wavelength and bandwidth, and high quantum efficiency are highly desirable in practice applications [3]. Thus, tailoring the emission property of a given phosphor to satisfy the above-mentioned properties is quite meaningful. Eu^{2+} is the most widely used activator due to its fast emission decay, broad-band, and highly efficient emission originating from $4f^7$-$4f^65d^1$ parity-allowed electric dipole transition [4,5]. Moreover, thanks to the outer extended 5d orbits, the energy state of $4f^65d^1$ level is strongly dependent on local surroundings around Eu^{2+}, thus by careful controlling over the magnitude of crystal field splitting, local site symmetry, activator-ligand bond covalency, fascinating emission colors can be intentionally achieved [6–8]. In those regards, many strategies such as neighboring-cation/anion substitution [9,10], chemical unit co-substitution [11], crystal-site engineering, and so on have been proposed to tune Eu^{2+} photoluminescence [12,13]. Among these, crystal-site engineering is one of the most effective ways, which requires that the host contains at least two crystallographic independent doping sites. By controlling the site occupancy, we can achieve desired emission properties and therefore broadening the application of the phosphor.

In 2014, Kakihana et al. found that by simply increment the doping level of Eu^{2+}, the Eu^{2+} can be entered from a large Ca(1n) site to a smaller Ca(2n) site in $Ca_2SiO_4:Eu^{2+}$, correspondingly, red-shifting the emission color from yellow to ideal red spectrum region [14]. Undoubtedly, a host contains more potential doping sites, where there shall be a wider tunable emission color range. Based on this concern, we focused on $Ba_3MB_3O_9$ (M = Dy, Ho, Y, Er, Tm, Yb, Lu, and Sc) host, for it possesses abundant cationic sites [15,16]. $Ba_3MB_3O_9$ belongs to the big family of borates and possesses layered-type structures [17]. They are ideal phosphor host candidates and receives enormous attention in recent years. For example, Li's group reported orange $Ba_3ScB_3O_9:Eu^{2+}$ phosphor with a dual-emission band at 560 nm and 670 nm [18]. Wang's group reported the $Ba_3ScB_3O_9:Eu^{2+}$ can emit near infrared (NIR) light with a single emission peak at 736 nm. Strikingly, both of them attributed the emission to the Eu^{2+} ion occupying nine-fold coordinated Ba^{2+} sites (Eu_{Ba}), however, this is quite confusing, therefore, further investigations between Eu^{2+} luminescence mechanisms should be done [19]. Moreover, the previous researches didn't report the tunable emission from yellow to NIR in $Ba_3ScB_3O_9:Eu^{2+}$, which is quite important not only for broadening the application of the phosphor but also for understanding the intrinsic luminescence mechanisms.

Herein, Eu^{2+} doped $Ba_3ScB_3O_9$ phosphor was prepared, and

* Corresponding author.
E-mail address: xiazg@scut.edu.cn (Z. Xia).

https://doi.org/10.1016/j.physo.2021.100077
Received 22 April 2021; Received in revised form 1 June 2021; Accepted 1 June 2021
Available online 4 June 2021

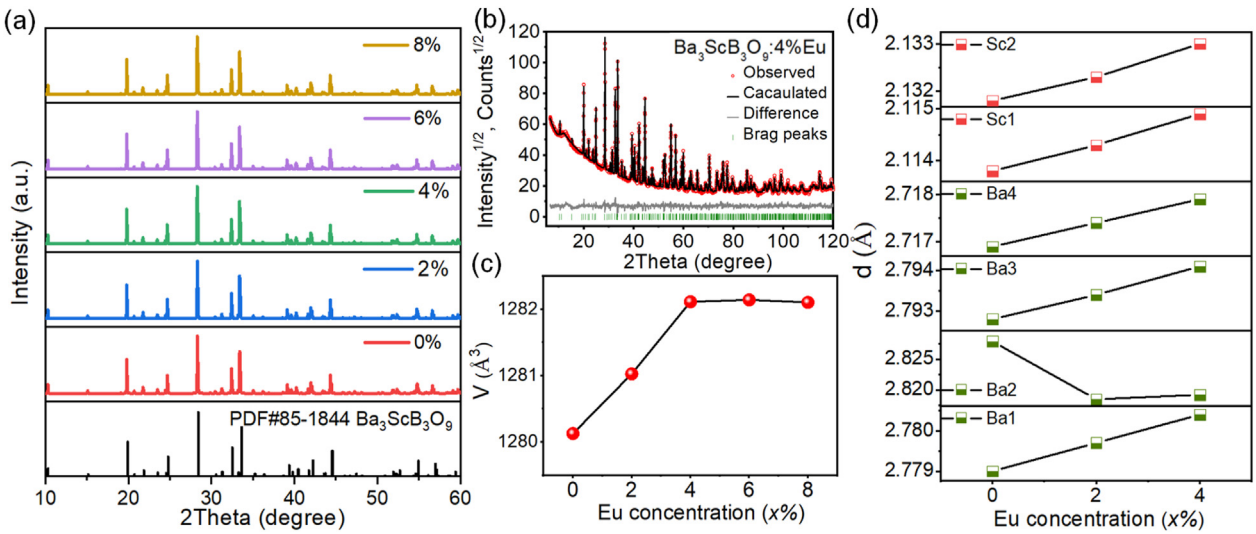

Fig. 1. **a.** X-ray powder diffraction patterns of $Ba_3ScB_3O_9$:*x*Eu (x = 0%–8%). **b.** Rietveld refinement of $Ba_3ScB_3O_9$:4%Eu. **c.** Cell volume V(x) dependence of the Eu doping concentration (x = 0%–8%). **d.** Dependence of the average bond length of Ba and Sc in $Ba_3ScB_3O_9$:*x*Eu (x = 0%–4%).

photoluminescence tuning was achieved by crystal-site engineering. We demonstrate that the emission color of the phosphor can be widely tuned from NIR to yellow by chemically driving the Eu^{2+} from octahedrally-coordinated Sc^{3+} sites to nine-fold coordinated Ba^{2+} sites. On the basis of the detailed analysis of the relationship between emission characteristics and the local environment of Eu^{2+} ions, the occupation mechanism of Eu^{2+} has been elaborated. Our research will initiate and guide more exploration on discovering new phosphors through crystal-site engineering.

2. Material and methods

2.1. Sample preparation

Eu^{2+}-doped $Ba_3ScB_3O_9$ samples were prepared by the traditional high-temperature solid-state reaction method. According to the given compositions, the stoichiometry contents of raw materials $BaCO_3$ (AR), H_3BO_3 (AR), Sc_2O_3 (99.99%), and Eu_2O_3 (99.99%) were weighed and ground in an agate of about 1 h for full mixing. To compensate the volatilization, the amount of H_3BO_3 was slightly excessed. Then these uniform mixtures were put in the alumina crucibles and sintered at around 1150 °C for 6 h in a reducing mixed atmosphere of H_2 (20%) and N_2 (80%). After that, the furnace cooled down naturally to room temperature, and the sintered samples were ground again for further characterization.

Table 1
Main parameters of processing and refinement of the $Ba_3ScB_3O_9$:*x*Eu samples.

x (%)	Space Group	Cell parameters (Å), Cell Volume (Å^3)	R_{wp}, R_p, R_B, χ^2
0	$P6_3cm$	a = 9.2836 (1), c = 17.1521 (2), V = 1280.20 (3)	6.91, 5.01, 3.45, 1.71
2	$P6_3cm$	a = 9.28465 (12), c = 17.1568 (3), V = 1280.85 (4)	6.33, 4.63, 3.06, 1.60
4	$P6_3cm$	a = 9.28649 (13), c = 17.1658 (3), V = 1282.03 (4)	5.69, 4.20, 2.42, 1.68

2.2. Characterization

XRD was performed via an Aeris X-ray diffractometer (PANalytical Corporation, Netherlands) at 40 kV and 15 mA with monochromatized Cu Kα radiation (λ = 1.5406 Å). The Rietveld structure refinements were performed using TOPAS 4.2 [20]. The PL, PLE spectra, temperature-dependent emission spectra, and luminescence decay curves were obtained using an Edinburgh FLS1000 fluorescence spectrophotometer.

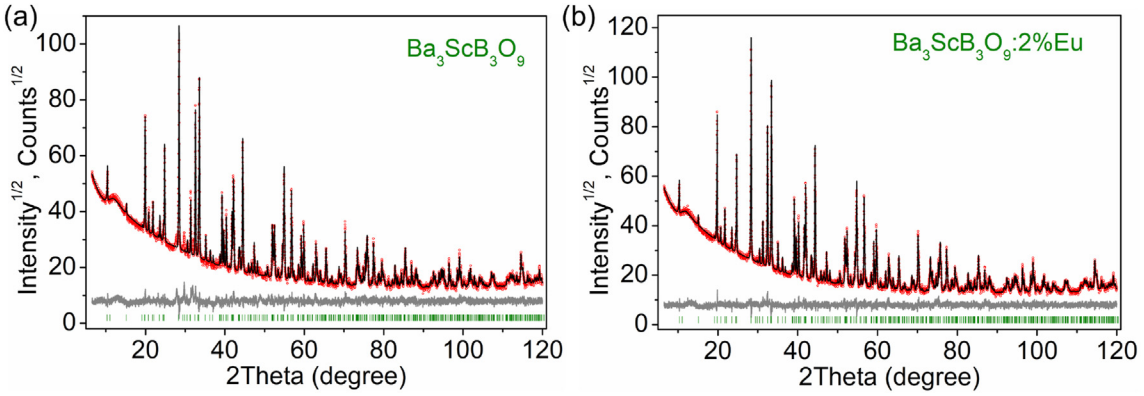

Fig. 2. Rietveld refinement of $Ba_3ScB_3O_9$ and $Ba_3ScB_3O_9$:2%Eu. The solid black lines are the calculated intensities, and the red dots are the observed intensities. The gray solid lines below the profiles stand for the difference between the observed and calculated intensities. The short green vertical lines show the position of the Bragg reflections of the calculated $Ba_3ScB_3O_9$. (For interpretation of the references to color in this figure legend, the reader is referred to the Web version of this article.)

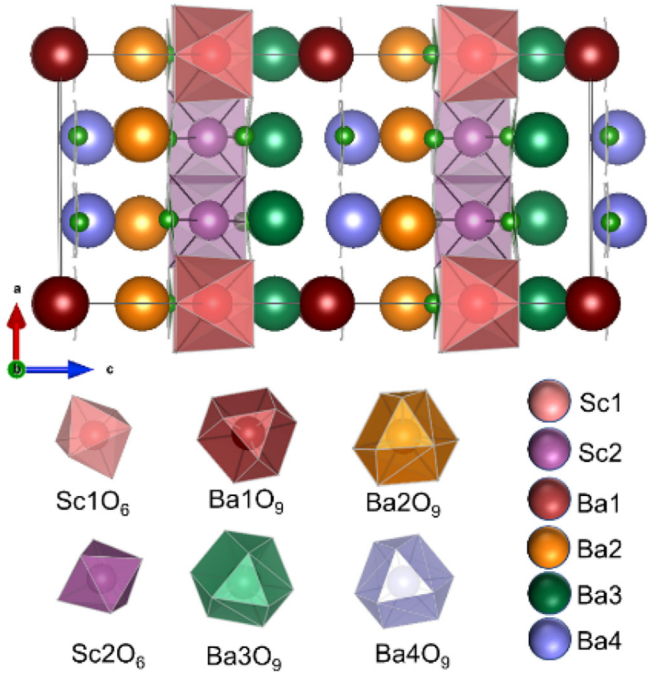

Fig. 3. Crystal structure of $Ba_3ScB_3O_9$ and polyhedral geometry of $Sc1O_6$, $Sc2O_6$, $Ba1O_9$, $Ba2O_9$, $Ba3O_9$, and $Ba4O_9$.

The low-temperature PL spectra and decay curves were recorded on an Edinburgh FLS920 fluorescence spectrophotometer using a liquid helium cooling reagent. The emission and excitation monochromator slits were set to minimal to reduce the instrumental resolution, with a 0.05 nm wavelength resolution.

3. Results and discussions

XRD patterns of $Ba_3ScB_3O_9$:xEu^{2+} (x = 0%–8%) phosphors are presented in Fig. 1a. The diffraction peaks of samples can be well indexed with the standard data of $Ba_3ScB_3O_9$ (PDF No.85-1844) which belongs to the *P6₃cm* space group and no impurities were observed. To further understand the phase structure and occupation mechanism of Eu^{2+} ions, Rietveld refinement was performed as shown in Figs. 1b and 2. Moreover, Table 1 listed the specific parameters of the studied phases for comparison. In the $Ba_3ScB_3O_9$ host (**Fig. 3**), there are four distinct Ba sites with a coordination number of 9 and two Sc sites with 6-fold coordination. These BaO_9 polyhedrons and ScO_6 octahedrons build a dense three-dimensional network structure by sharing the edges, and faces. The B atoms, filled in the interstitial sites, are coordinated with three oxygen atoms and are shared with BaO_9 polyhedrons. The Eu^{2+} ion can potentially locate in any site except B. The cell volume increasing firstly with x in the range of 0%–4% (**Fig. 1c**) indicates that the Eu^{2+} should mainly occupy Sc sites since the ionic radius of Eu^{2+} are bigger than the Sc^{3+} ion and smaller than Ba^{2+}. Also, some parts of the Eu^{2+} ion can be located in Ba sites since the cell volume keeping almost constant as x increasing between 4% and 8%. To further analyze the Eu^{2+} site occupation, Fig. 1d illustrates the average bond lengths of several polyhedrons in different concentrations of Eu^{2+} doped $Ba_3ScB_3O_9$ by extracting the data from Rietveld refinement. As we can see, the Sc1-O and Sc2-O average bond lengths increase with Eu^{2+} doping concentration increase from 0% to 4%. This result further supports $Eu^{2+} \leftrightarrow Sc^{3+}$ replacement. However, the Ba–O average bond lengths shows different line trends upon Eu^{2+} doping, where Ba2–O decreased, Ba1–O, Ba3–O and Ba4–O increased. Considering the ionic radius of Eu^{2+} and Ba^{2+}, we propose that Eu^{2+} occupies only at the Ba2 site due to $Eu^{2+} \leftrightarrow Ba^{2+}$ replacement would shorter Ba–O bond length. The abnormal prolonged Ba1–O, Ba3–O and Ba4–O bond lengths are possibly due to the slight distortion of the lattice caused by $Eu^{2+} \leftrightarrow Sc^{3+}$ replacement.

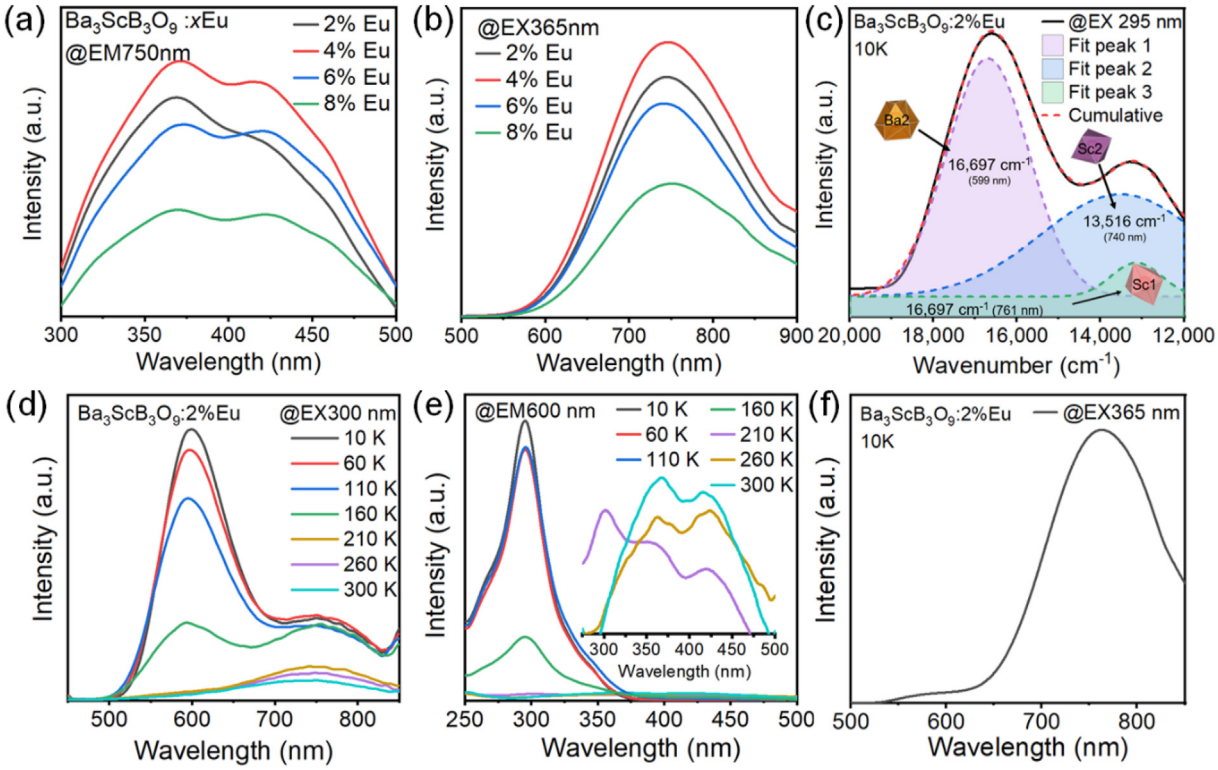

Fig. 4. a PLE and **b.** PL spectra of $Ba_3ScB_3O_9$:xEu (x = 0%–8%) monitored/measured at 750 and 365 nm. **c.** The emission spectrum and Gaussian fitting curves of $Ba_3ScB_3O_9$:2%Eu measured at 295 nm in 10 K. **d.** PL and **e.** PLE spectra of $Ba_3ScB_3O_9$:2%Eu measured/monitored at 300 and 600 nm in 10–300 K at intervals of 50 K. **f.** PL spectra of $Ba_3ScB_3O_9$:2%Eu measured at 365 nm in 10 K.

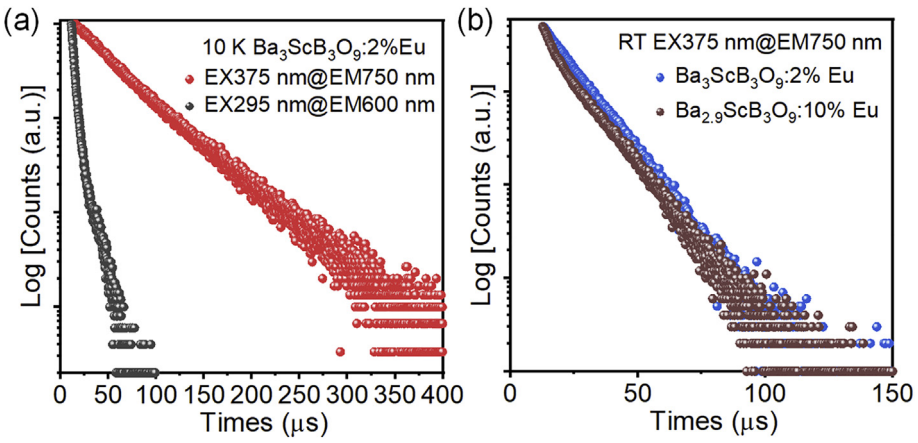

Fig. 5. a. Decay curves of $Ba_3ScB_3O_9$:2%Eu monitored at different excitation and emission wavelengths in 10 K. b. Decay curves of $Ba_3ScB_3O_9$:2%Eu and $Ba_{2.9}ScB_3O_9$:10%Eu under the excitation of 375 nm and monitored at 750 nm in RT.

When Eu^{2+} doping concentration is higher than 4%, the cell volume almost remains unchanged, indicating that the content of Eu^{2+} in the system probably reaches saturation. And it is worth noting that Eu^{2+} and Sc^{3+} not only have a large difference in ion radius but also have different valence states, so the concentration of Eu^{2+} ion replacing the Sc^{3+} site is limited. Based on the above results, one can conclude that the main occupation mechanism is ascribed to $Eu^{2+} \rightarrow Sc^{3+}$ replacements (Eu_{Sc1} Eu_{Sc2}), while a small amount of Eu^{2+} located in the Ba2 site (Eu_{Ba2}).

Fig. 4a and **b** gives the room temperature photoluminescence emission (PL) and excitation (PLE) spectra of $Ba_3ScB_3O_9$:*x*Eu (x = 0%–8%), respectively. When monitored at 750 nm, $Ba_3ScB_3O_9$:*x*Eu (x = 0%–8%) gives an ultra-broad excitation band that nearly covered the full ultraviolet and blue regions. Such a broad excitation band should be ascribed to the 4f → 5d transition of Eu^{2+} and would favors its application for ultraviolet and blue light-pumped pc-LEDs. As shown in Fig. 4b, under 365 nm excitation, the phosphors exhibit similar broadband NIR emission centered at around 750 nm with an almost identical FWHM of 190 nm. And the intensity of $Ba_3ScB_3O_9$:4%Eu^{2+} phosphor is strongest, beyond the concentration, the concentration quenching effect would weaken the NIR emission originating from the typical 5d → 4f transition of Eu^{2+} occupying at Sc site as we verified by structural analysis. Noteworthy, it is usually reckoned that Eu^{2+} is difficult to replace trivalent rare-earth ions because of the large difference in valence state and radius between them. However, the emission of Eu at trivalent rare-earth sites has been reported recently, and some previous researchers do hard work on the blue emission of Eu^{2+} doped $Y_3Al_5O_{12}$ (YAG) phosphor [21,22]. And our group also discover some phosphors like $A_3LnSi_2O_7$:Eu^{2+} [23, 24] and $Sr_3LnAl_2O_{7.5}$:Eu^{2+} [25] (A = K, Rb; Ln = Y or Lu), which enable deep-red emission originating from Eu^{2+} at the Y and Lu sites [26,27]. With the change of doping concentration, the luminescence intensity reaches its maximum value when x is 4%, and then decreases as x continues to increase. The peak and shape of the emission band do not change significantly, which is consistent with the previous structural analysis as x is greater than 4%, the Eu^{2+} content in $Ba_3ScB_3O_9$ reaches saturation. And the changing trend of excitation spectrum is consistent with it.

The asymmetric spectral profile demonstrates that there exists more than one luminescent center in $Ba_3ScB_3O_9$:Eu. To verify this point, the low-temperature PLE/PL spectra from 10 K to 300 K are measured. As is shown in Fig. 4f, $Ba_3ScB_3O_9$:2%Eu exhibits bimodal emission under the 365 nm excitation in 10 K. In addition to the near-infrared emission peak around 750 nm, a yellow emission peak also exists around 600 nm. The further study on the low-temperature yellow emission, as shown in Fig. 4e, the excitation spectrum monitored at 600 nm in 10 K can only observe a sharp peak around 300 nm, with the increase of temperature, its intensity decreases. While in the range of 300 nm–500 nm it exists a significant peak, and its shape with the near-infrared spectrum corresponding excitation peak shape similarity. The same phenomenon can be observed from the low-temperature emission spectrum, even in 10 K, and the near-infrared emission peak can still be observed. With increasing temperature, the intensity of the yellow emission peak decreases until no obvious emission peak can be observed.

The emission band upon the excitation of 295 nm in 10 K is exactly deconvoluted into three Gaussian spectral profiles with three peaks at 16,697 cm^{-1} (599 nm), 13,516 cm^{-1} (740 nm), and 13,137 cm^{-1} (761 nm), suggesting that it exists three different luminescence centers in $Ba_3ScB_3O_9$ (**Fig. 4c**). This conclusion is consistent with the above structural studies, and the three luminescence centers should correspond to the three sites Eu_{Ba2}, Eu_{Sc1}, and Eu_{Sc2}. It is well-known that the 5d energy-level position of Eu^{2+} is strongly affected by the crystal-field strength from its original location of 4.2 eV (34,000 cm^{-1}), which usually leads to a red-shift emission of Eu^{2+}. The following equation proposed by Van Uitert can be used to appraise the red-shift degree of Eu^{2+} in different coordination environments [28]:

$$E = Q[1 - (\frac{V}{4})^{\frac{1}{V}} \times 10^{-nE_a r/80}] \quad (1)$$

In this equation, E stands for the d-band-edge position of an activated ion (Eu^{2+}) in a phosphor, Q denotes the d-band-edge position of a free ion (34,000 cm^{-1} for Eu^{2+}), V denotes the valence of active ion (V = 2 for Eu^{2+}), n represents the coordination number of the activator, E_a refers to the electron affinity of the anion atoms, always be constant in a host material, and r stands for the substituted ion radius in the host lattice. Namely, the emission position (E) is proportional to the factors n and r. Hence, we conclude that the emission peak at 600 nm belongs to Eu_{Ba2}. Under this circumstance, the emission positions of Eu_{Sc1} and Eu_{Sc2} are still unclear. As $Sc1O_6$ and $Sc2O_6$ have the same coordination number and similar polyhedron shapes, the centroid shift and Stokes shift would have a similar effect on the emission of Eu_{Sc1} and Eu_{Sc2}. And the crystal field splitting depends especially on the distortion of the coordination environment, so that we use the energy-level separation (D_q) to compare it in Eu_{Sc1} and Eu_{Sc2} [29]:

$$D_q = \frac{1}{6} Ze^2 \frac{r^4}{R^5} \quad (2)$$

here, Z stands for the anion charge, e is a constant of electron charge, r represents the average value of the d electron radial coordinate, and R stands for the practical bond length. It is obvious that the crystal field splitting is inversely proportional to R^5, the R values of Sc1-O and Sc2-O in $Ba_3ScB_3O_9$ are 2.11 Å and 2.13 Å. In that way, the emission peak at 761 nm belongs to Eu_{Sc} and the one at 740 nm belongs to Eu_{Sc1}.

To better understand the existence of multiple emitting centra in

Table 2
Lists of the luminescent decay times (τ_1, τ_2, τ_3), fitting constants (A_1, A_2, A_3), average decay times (τ_{ave}) during the fitting of the decay curves of $Ba_3ScB_3O_9$:2%Eu and $Ba_{2.9}ScB_3O_9$:10%Eu at different temperature.

$Ba_3ScB_3O_9$:2%Eu, 10 K								
λ_{ex} (nm)	λ_{em} (nm)	A_1	τ_1 (μs)	A_2	τ_2 (μs)	A_3	τ_3 (μs)	τ_{ave} (μs)
375	750	4140.49	44.24	–	–	–	–	44.24
295	600	116908.23	2.81	136.41	16.78	–	–	2.91
$Ba_3ScB_3O_9$:2%Eu, Room Temperature								
375	750	6039.40	5.19	12476.22	12.65	–	–	11.41
$Ba_{2.9}ScB_3O_9$:10%Eu, Room Temperature								
365	577	3610.07	0.19	1900.34	0.86	1565.3	2.69	1.97
375	750	65681.41	3.75	7336.23	13.34	–	–	6.48

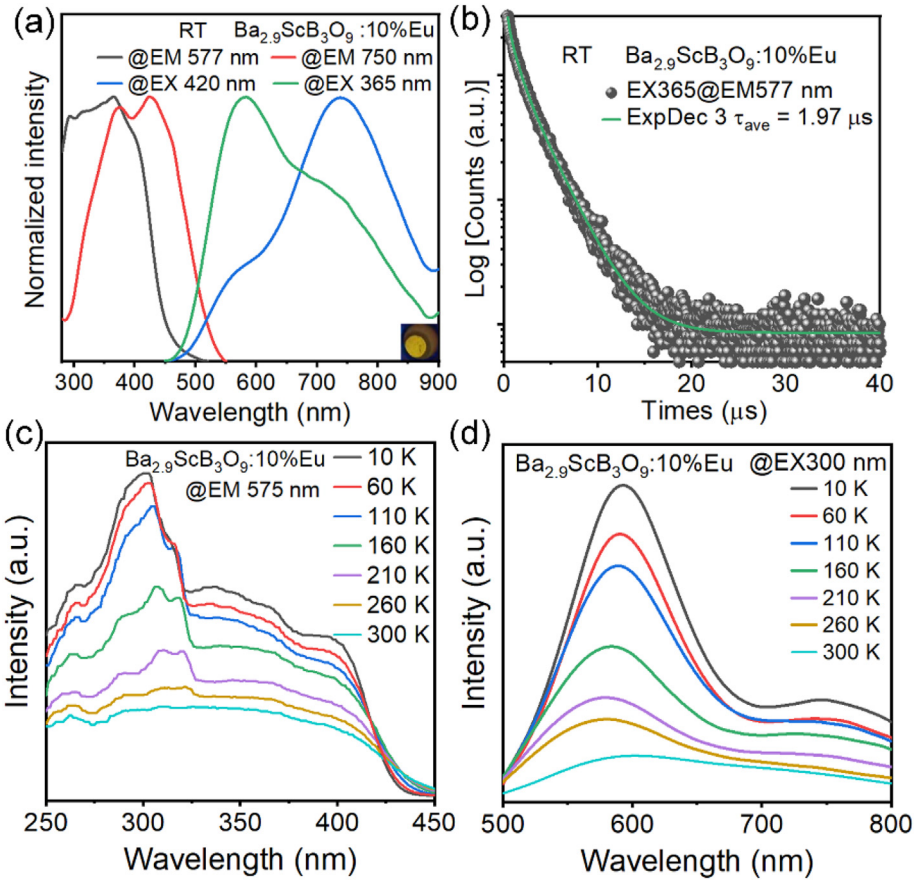

Fig. 6. a. PLE and PL spectra of $Ba_{2.9}ScB_3O_9$:10%Eu made in different condition. b. Decay curves of $Ba_{2.9}ScB_3O_9$:10%Eu under the excitation of 365 nm and monitored at 577 nm in RT. c. PLE and d. PL spectra of $Ba_{2.9}ScB_3O_9$:10%Eu monitored/measured at 575 and 300 nm in 10–300 K at intervals of 50 K.

$Ba_3ScB_3O_9$:2%Eu, the fluorescence decay curves of the sample were monitored at different excitation and emission wavelengths in 10 K. The decay curves were comparatively fitted by mono- ($n = 1$), bi- ($n = 2$) and triple-($n = 3$) exponential functions [30]:

$$I = \sum_{i=1}^{n} A_i exp(-\frac{t}{\tau_i}) \ (n = 1, 2, 3) \quad (3)$$

where I denotes luminescence intensity, t represents time, τ_i is the lifetime for different components; and A_i is the corresponding fitting constants. As compared in Fig. 5a, the decay curve measured at 600 nm emission and 295 nm excitation, can be well fitted by the bi-exponential function whose average lifetime values are 2.91 μs. The decay curves measured at 750 nm emission and 375 nm excitation can be fitted by the mono-exponential function whose average lifetime values are 44.24 μs. The detailed fitting results are presented in Table 2. The mono-exponential fitting supports the fact that the two sub-Gaussian bands with lower intensity are almost overlapped. And, the long decay time would be related to the fact that the radiation decay rate of a transition is proportional to the energy to the power 3 [31], and low temperature would let the decay time longer, so it is reasonable that the Eu^{2+} emission in $Ba_3ScB_3O_9$ has a larger decay value. The two completely different fluorescence decay curves indicate multiple Eu^{2+}-emitting centers in $Ba_3ScB_3O_9$:2%Eu phosphor.

In $Ba_3ScB_3O_9$:*x*Eu phosphors, the maximum Eu^{2+} doping concentration is limited, and only a small amount of Eu^{2+} is introduced into Ba2 site, which limits the photoluminescence tuning. In order to increase the doping content of Eu^{2+}, one can explore useful strategies to promote more Eu^{2+} enter the Ba site to discover phosphors with different luminescence phenomena. A new phosphor, $Ba_{2.9}ScB_3O_9$:10%Eu, was designed by reducing the content of Ba and increasing the content of Eu. The XRD refinement results on $Ba_{2.9}ScB_3O_9$:10%Eu showed that the phosphor is almost pure phase with only a tiny of insignificant impurity.

$Ba_{2.9}ScB_3O_9$:10%Eu can emit a completely different yellow light from $Ba_3ScB_3O_9$:2%Eu when irradiated by a 365 nm UV lamp at room temperature, suggesting the successful color point tuning via crystal-site engineering. As shown in Fig. 6a, under 365 nm excitation, $Ba_{2.9}ScB_3O_9$:10%Eu presents a broad emission across the green to the near-infrared light region, with the strongest peak located at about 580 nm and a shoulder peak around 750 nm. The corresponding decay curve of the NIR emission has been compared with $Ba_3ScB_3O_9$:2%Eu as shown in Fig. 5b, both of them have the same decay tendency, and the average lifetime value of $Ba_{2.9}ScB_3O_9$:10%Eu is 6.48 μs, which is shorter than the other average lifetime value 11.41 μs. It also indicates that through crystal-site engineering more Eu^{2+} ions have been driving from octahedrally-coordinated Sc^{3+} sites to nine-fold coordinated Ba^{2+} sites which result in a shorter lifetime. In addition, the completely different excitation spectra (Fig. 6a) corresponding to the two emission peaks at room temperature also proved it. Here, we focus on the emission peak around 580 nm. One can find from Fig. 6c that the temperature-dependent PLE spectra monitored at 575 nm appears more and more obvious small spikes at about 300 nm as temperature decrease from 300 K to 10 K, and its shape is completely different from that of $Ba_3ScB_3O_9$:2%Eu under the same condition. As illustrated in Fig. 6b, at room temperature, the fluorescence decay curves monitored at 365 nm excitation and 575 nm emission wavelengths can be well fitted by the triple-exponential function (The detailed fitting results are presented in Table 2) indicating it exists multiple luminescence centers. As four coordination polyhedrons of Ba is very similar, the replacement of Eu^{2+} would lead to similar emission which is difficult to be distinguished. Photoluminescence tuning from near-infrared light to yellow light is achieved by chemically driving the Eu^{2+} from nine-fold coordinated Ba^{2+} sites to octahedrally-coordinated Sc^{3+} site, while the mechanism of Eu^{2+} occupation in $Ba_{2.9}ScB_3O_9$:10%Eu needs to be further analyzed, which would have important guiding significance for the future discovery of new high-performance phosphors.

4. Conclusions

In summary, we successfully prepared $Ba_3ScB_3O_9$:*x*Eu NIR phosphors (FWHM = 190 nm, λ_{em} = 750 nm) with Eu^{2+} doping content *x* ranging from 2% to 8%. According to the structural and spectral analysis, the bright NIR emission is assigned to the prior occupation of Eu^{2+} in octahedrally-coordinated Sc1 and Sc2 sites. Therefore, Eu^{2+} suffers a large crystal field splitting, and shifts the emission energy into NIR region. Moreover, based on the crystal-site engineering approach, we have also designed a yellow emitting phosphor $Ba_{2.9}ScB_3O_9$:10%Eu. Results show that more Eu^{2+} ions can be driving from Sc sites into Ba sites with 9-fold coordination by simply decreasing Ba^{2+} content, which is responsible for the color points tuning. This work studies the mechanism of Eu^{2+} site occupation in $Ba_3ScB_3O_9$ and exploits a series of NIR/yellow phosphors which can be a promising component for future pc-LEDs lighting sources.

CRediT authorship contribution statement

Shunqi Lai: Writing – original draft, were responsible for the experiment. **Tao Hu:** discussed the results and revise the paper. **Maxim S. Molokeev:** performed the refinement. **Zhiguo Xia:** Project administration, conceived the project and revised the paper.

Declaration of competing interest

The authors declare that they have no known competing financial interests or personal relationships that could have appeared to influence the work reported in this paper.

Acknowledgments

The present work was supported by the National Natural Science Foundation of China (Grant Nos. 51972118 and 51961145101), International Cooperation Project of National Key Research and Development Program of China (2021YFE0105700), the Guangzhou Science & Technology Project (202007020005), and the Local Innovative and Research Teams Project of Guangdong Pearl River Talents Program (2017BT01X137). This work is also funded by RFBR according to the research project No. 19-52-80003.

References

[1] X. Zhou, J. Qiao, Z. Xia, Learning from mineral structures toward new luminescence materials for light-emitting diode applications, Chem. Mater. 33 (2021) 1083–1098, https://doi.org/10.1021/acs.chemmater.1c00032.
[2] J. Qiao, J. Zhao, Q. Liu, Z. Xia, Recent advances in solid-state LED phosphors with thermally stable luminescence, J. Rare Earths 37 (2019) 565–572, https://doi.org/10.1016/j.jre.2018.11.001.
[3] Z. Xia, Q. Liu, Progress in discovery and structural design of color conversion phosphors for LEDs, Prog. Mater. Sci. 84 (2016) 59–117, https://doi.org/10.1016/j.pmatsci.2016.09.007.
[4] X. Qin, X. Liu, W. Huang, M. Bettinelli, X. Liu, Lanthanide-activated phosphors based on 4f-5d optical transitions: theoretical and experimental aspects, Chem. Rev. 117 (2017) 4488–4527, https://doi.org/10.1021/acs.chemrev.6b00691.
[5] G. Li, Y. Tian, Y. Zhao, J. Lin, Recent progress in luminescence tuning of Ce^{3+} and Eu^{2+}-activated phosphors for pc-WLEDs, Chem. Soc. Rev. 44 (2015) 8688–8713, https://doi.org/10.1039/c4cs00446a.
[6] Z. Xia, K.R. Poeppelmeier, Chemistry-inspired adaptable framework structures, Acc. Chem. Res. 50 (2017) 1222–1230, https://doi.org/10.1021/acs.accounts.7b00033.
[7] S. Wang, Z. Song, Y. Kong, Q. Liu, Relationship of Stokes shift with composition and structure in Ce^{3+}/Eu^{2+}-doped inorganic compounds, J. Lumin. 212 (2019) 250–263, https://doi.org/10.1016/j.jlumin.2019.04.036.
[8] M.R. Amin, P. Strobel, A. Qamar, T. Giftthaler, W. Schnick, A. Moewes, Understanding of luminescence properties using direct measurements on Eu^{2+}-doped wide bandgap phosphors, Adv. Opt. Mater. (2020), https://doi.org/10.1002/adom.202000504, 2000504.
[9] X. Li, Z. Wang, J. Liu, X. Meng, K. Qiu, Q. Bao, Y. Li, Z. Wang, Z. Yang, P. Li, Mechanism of crystal structure transformation and abnormal reduction in $Ca_{5-y}(BO_3)_{3-x}(PO_4)_xF$ (CBP_xF): yBi^{3+}, Inorg. Chem. 57 (2018) 13783–13799, https://doi.org/10.1021/acs.inorgchem.8b02317.
[10] H. Wu, H. Li, L. Jiang, R. Pang, S. Zhang, D. Li, G. Liu, C. Li, J. Feng, H. Zhang, Design of a mixed-anionic-ligand system for a blue-light-excited orange-yellow emission phosphor $Ba_{1.31}Sr_{3.69}(BO_3)_3Cl:Eu^{2+}$, J. Mater. Chem. C 8 (2020) 3040–3050, https://doi.org/10.1039/c9tc06360a.
[11] Z. Xia, C. Ma, M.S. Molokeev, Q. Liu, K. Rickert, K.R. Poeppelmeier, Chemical unit cosubstitution and tuning of photoluminescence in the $Ca_2(Al_{1-x}Mg_x)(Al_{1-x}Si_{1+x})O_7$:$Eu^{2+}$ phosphor, J. Am. Chem. Soc. 137 (2015) 12494–12497, https://doi.org/10.1021/jacs.5b08315.
[12] M. Zhao, Z. Xia, M.S. Molokeev, L. Ning, Q. Liu, Temperature and Eu^{2+}-doping induced phase selection in $NaAlSiO_4$ polymorphs and the controlled yellow/blue emission, Chem. Mater. 29 (2017) 6552–6559, https://doi.org/10.1021/acs.chemmater.7b02548.
[13] L. He, Z. Song, X. Jia, Z. Xia, Q. Liu, Consequence of optimal bonding on disordered structure and improved luminescence properties in T-phase $(Ba,Ca)_2SiO_4:Eu^{2+}$ phosphor, Inorg. Chem. 57 (2018) 4146–4154, https://doi.org/10.1021/acs.inorgchem.8b00362.
[14] Y. Sato, H. Kato, M. Kobayashi, T. Masaki, D.H. Yoon, M. Kakihana, Tailoring of deep-red luminescence in $Ca_2SiO_4:Eu^{2+}$, Angew. Chem. Int. Ed. 53 (2014) 7756–7759, https://doi.org/10.1002/anie.201402520.
[15] T.N. Khamaganova, Structural specific features and properties of alkaline earth and rare earth metal borates, Russ. Chem. Bull. 66 (2017) 187–200, https://doi.org/10.1007/s11172-017-1719-6.
[16] D.A. Keszler Anthony Diaz, Eu^{2+} luminescence in the borates $X_2Z(BO_3)_2$ (X = Ba, Sr; Z = Mg, Ca), Chem. Mater. 9 (1997) 2017–2077, https://doi.org/10.1021/cm9700817.
[17] James R. Cox, Douglas A. Keszler, J. Huang, The layered borates $Ba_3M(B0\text{-}_3)_3$ (M = Dy, Ho, Y, Er, Tm, Yb, Lu, and Sc), Chem. Mater. 6 (1994) 2008–2013, https://doi.org/10.1021/cm00047a021.
[18] D. Zhang, G. Li, Z. Leng, L. Li, Site occupancy and tunable photoluminescence properties of Eu^{2+}-activated $Ba_3Sc(BO_3)_3$ phosphors for white light emitting diodes, J. Alloys Compd. 815 (2020), https://doi.org/10.1016/j.jallcom.2019.152645, 152645.
[19] Z. Tang, Q. Zhang, Y. Cao, Y. Li, Y. Wang, Eu^{2+}-doped ultra-broadband VIS-NIR emitting phosphor, Chem. Eng. J. 388 (2020), https://doi.org/10.1016/j.cej.2020.124231, 124231.
[20] Bruker, AXS TOPAS V4, General Profile and Structure Analysis Software for Powder Diffraction Data. – User's Manual, Bruker AXS, Karlsruhe, Germany, 2008.
[21] Q.Q. Zhu, W.W. Hu, L.C. Ju, L.Y. Hao, X. Xu, S. Agathopoulos, B. Karmakar, Synthesis of $Y_3Al_5O_{12}:Eu^{2+}$ phosphor by a facile hydrogen iodide-AssistedSol-gel method, J. Am. Ceram. Soc. 96 (2013) 701–703, https://doi.org/10.1111/jace.12222.

[22] L. Havlák, J. Bárta, M. Buryi, V. Jarý, E. Mihóková, V. Laguta, P. Boháček, M. Nikl, Eu^{2+} stabilization in YAG structure: optical and electron paramagnetic resonance study, J. Phys. Chem. C 120 (2016) 21751–21761, https://doi.org/10.1021/acs.jpcc.6b06397.

[23] J. Qiao, M. Amachraa, M. Molokeev, Y.-C. Chuang, S.P. Ong, Q. Zhang, Z. Xia, Engineering of $K_3YSi_2O_7$ to tune photoluminescence with selected activators and site occupancy, Chem. Mater. 31 (2019) 7770–7778, https://doi.org/10.1021/acs.chemmater.9b02990.

[24] J. Qiao, L. Ning, M.S. Molokeev, Y.C. Chuang, Q. Zhang, K.R. Poeppelmeier, Z. Xia, Site-selective occupancy of Eu^{2+} toward blue-light-excited red emission in a $Rb_3YSi_2O_7$:Eu phosphor, Angew. Chem. Int. Ed. 58 (2019) 11521–11526, https://doi.org/10.1002/anie.201905787.

[25] T. Hu, Y. Gao, M.S. Molokeev, Z. Xia, Q. Zhang, Eu^{2+} stabilized at octahedrally coordinated Ln^{3+} site enabling red emission in $Sr_3LnAl_2O_{7.5}$ (Ln = Y or Lu) phosphors, Adv. Opt. Mater. (2021), https://doi.org/10.1002/adom.202100077, 2100077.

[26] J. Qiao, G. Zhou, Y. Zhou, Q. Zhang, Z. Xia, Divalent europium-doped near-infrared-emitting phosphor for light-emitting diodes, Nat. Commun. 10 (2019) 5267, https://doi.org/10.1038/s41467-019-13293-0.

[27] Y. Pan, X. Xie, Q. Huang, C. Gao, Y. Wang, L. Wang, B. Yang, H. Su, L. Huang, W. Huang, Inherently Eu^{2+}/Eu^{3+} codoped Sc_2O_3 nanoparticles as high-performance nanothermometers, Adv. Mater. 30 (2018), https://doi.org/10.1002/adma.201705256 e1705256.

[28] L.G.V. Uitert, An empirical relation fitting the position in energy of the lower d-band edge for Eu^{2+} or Ce^{3+} in various compounds, J. Lumin. 29 (1984) 1–9, https://doi.org/10.1016/0022-2313(84)90036-X.

[29] A.B.P. Lever, The crystal field splitting parameter dq: calculation and significance, Adv. Chem. 62 (1967) 430–451, https://doi.org/10.1021/ba-1967-0062.ch029.

[30] J. Qiao, L. Ning, M.S. Molokeev, Y.C. Chuang, Q. Liu, Z. Xia, Eu^{2+} site preferences in the mixed cation $K_2BaCa(PO_4)_2$ and thermally stable luminescence, J. Am. Chem. Soc. 140 (2018) 9730–9736, https://doi.org/10.1021/jacs.8b06021.

[31] S.H.M. Poort, A. Meyerink, G. Blasse, Lifetime measurements in Eu^{2+}-doped host lattices, J. Phys. Chem. Solid. 58 (1997) 1451–1456, https://doi.org/10.1016/S0022-3697(97)00010-3.